Carbohydrate Polymers 102 (2014) 489–496

Contents lists available at ScienceDirect

Carbohydrate Polymers

journal homepage: www.elsevier.com/locate/carbpol

Metal ion induced-assembly of amylose in aqueous solution

Yinhui Li[a,b,c], Shudong Lin[a,b], Jiwen Hu[a,b,*], Guojun Liu[a,d], Gangwei Zhang[a,b], Yuanyuan Tu[a,b], Hongsheng Luo[a,b], Wei Li[a,b]

[a] Guangzhou Institute of Chemistry, Chinese Academy of Sciences, Guangzhou 510650, People's Republic of China
[b] Key Laboratory of Cellulose Lignocellulosics Chemistry, Chinese Academy of Sciences, 510650, People's Republic of China
[c] Engineering Research Center of Seawater Utilization Technology, Ministry of Education, School of Marine Science and Engineering, Hebei University of Technology, Tianjin, People's Republic of China
[d] Department of Chemistry, Queen's University, 90 Bader Lane, Kingston, Ontario, Canada K7L 3N6

ARTICLE INFO

Article history:
Received 23 October 2013
Accepted 27 November 2013
Available online 7 December 2013

Keywords:
Starch
Amylose
Metal ion
Induced-assembly

ABSTRACT

Cu^{2+}/amylose assemblies of various sizes were prepared through the Cu^{2+} ion induced-assembly of amylose. These assembly structures were characterized via transmission electronic microscopy (TEM), scanning electronic microscopy (SEM), dynamic light scattering (DLS), ^1H NMR analysis, fluorescence spectroscopy (FL) and UV–vis absorption spectroscopy (UV–vis). The results from these characterizations revealed the existence of a complexation effect and/or a bridging effect between the hydroxyl groups of amylose and Cu^{2+} ions, and that the formation of the hydrophobic domains promoted the formation of Cu^{2+}/amylose assemblies. The use of other metal ions to induce the formation of spherical, flower- and wire-like amylose assemblies was investigated as well. A preliminary investigation on the ability of amylose to capture various metal ions was also performed, and the results of this work demonstrated that amylose could bind quantitatively metal ions that were at low concentrations. This work provided an alternative strategy for the recovery of precious metals from metal ion-containing aqueous solutions and the reduction of water pollution.

1. Introduction

The field of polymer self-assembly holds great promise, and has attracted extensive interest in recent decades. Self-assembled polymers have been widely used as multi-functional polymeric materials fields for various applications, including drug release, catalysis, biomimetics, nano-devices, functional proteins, heavy metal absorbent materials, and for various other applications (Brown, Aksay, Saville, & Hecht, 2002; Moffitt & Eisenberg, 1997; Perez, Simeone, Saeki, Josephson, & Weissleder, 2003; Rosler, Vandermeulen, & Klok, 2001; Shen, Zhang, & Eisenberg, 1999; Sheparovych et al., 2006; Wang, Tang, Li, & Wang, 2009; Wen, Cao, Wang, Chen, & Luo, 2011; Xu, Ji, Chen, & Shen, 2005; Zhang & Eisenberg, 1996; Zhang et al., 2006). In a typical induced-assembly process, polymers tend to assemble and form fixed structures under certain external driving forces, such as changes to the pH (Shen et al., 1999), the presence of metal ions (Sheparovych et al., 2006; Zhang & Eisenberg, 1996) the use of templates (Brown et al., 2002), and various other external stimuli.

Research on metal ion-induced assembly began with the self-assembly of polypeptides and the development of supramolecular chemistry in the 1970s. The metal ion-induced assembly of polypeptide was initially investigated with the aim of designing multi-functional protein on demand. Since the 1990s, studies on metal ion-induced assembly have also been extended to block copolymers and proteins. Because they incorporated $-NH_2$ or $-COOH$ groups that could readily undergo complexation, these copolymers were capable of coordinating with metal ions, leading to the formation of polymeric assemblies with a great morphological diversity. There has been an abundance of literature describing the formation of polymer assemblies in the presence of metal ions. The metal-ion induced assembly of block copolymers was first reported by Zhang, Yu, and Eisenberg (1996). In their studies, the diblock copolymer poly(styrene-*b*-oxyethylene) assembled into rod-like micelles in block selective solvents. Meanwhile, the addition of Li^+ induced these structures to undergo a morphological transition to form flake-like assemblies. Similar phenomena were also observed among ionic and non-ionic copolymers. The inducing effect of the metal ions on the assembly of these copolymers was attributed to the binding or bridging interactions between the ions and the copolymers. Li, Gong, and Nakashima (2002) investigated

* Corresponding author at: Key Laboratory of Cellulose Lignocellulosics Chemistry, Chinese Academy of Sciences, 510650, People's Republic of China.
Tel.: +86 20 85232136; fax: +86 20 85232136.
E-mail address: hjw@gic.ac.cn (J. Hu).

0144-8617/$ – see front matter © 2013 Elsevier Ltd. All rights reserved.
http://dx.doi.org/10.1016/j.carbpol.2013.11.062

the alkali ion induced-assembly behavior of poly(ethylene oxide-*b*-methacrylic acid) (PEO-*b*-PMA) by employing the PMA-metal ion complex as the core and hydrophobic PEO block as the corona.

Investigations on the metal ion induced-assembly of polymers have been extended from synthetic polymers to natural polymers in recent years. Starch is a renewable resource that is readily available and affordable. In addition, starch has a wide range of practical applications in various fields (Miles, Morris, Orford, & Ring, 1985). There are two types of starches, including linear and branched starch. The former is also named amylose, and consists of glucose residues that are connected via beta-1,4-glycosidic bonds in a linear screw-like structure. Meanwhile, branched starch consists of 24–30 glucose residues that are connected via alpha-1,4-glycosidic bonds in an end-to-end manner. Amylose is fully soluble in hot water due to the large number of hydroxyl groups contained in the glucose residues. According to recent reports, the hydroxyl groups of starch have been used by various researchers to construct amphiphilic polymers by introducing hydrophobic groups or hydrophobic polymer chains into the main chains, which facilitated assembly of the starch derivative in aqueous solutions (Akiyoshi, Maruichi, Kohara, & Kitamura, 2002; Besheer, Hause, Kressler, & Mader, 2007; Han, Borjihan, Bai, Chen, & Jing, 2008; Ju, Yan, & Zhang, 2012; Morimoto, Ogino, Narita, Kitamura, & Akiyoshi, 2007; Tan et al., 2009; Tan, Xu, Li, Sun, & Wang, 2010). For example, Mäder et al. reported the assembly behavior of hydroxyethyl starch, which had been modified with various organic acids. The polymer was initially dissolved in THF before water was added, which served as a good solvent for the hydroxyethyl starch backbone and as a poor solvent for the organic acid segments. Consequently, the polymer underwent self-assembly to yield vesicles (Besheer et al., 2007).

Although the assembly of starch through the introduction of hydrophobic groups and polymer chains has been widely investigated, the metal ions induced-assembly of amylose has never been reported so far. Herein, we describe the use of metal ions to induce the self-assembly of water-soluble amylose chains through a complexation effect or bridging effect to yield polymeric assemblies with various sizes and morphologies. In addition, we have preliminarily studied the ability of amylose to capture trace metal ions from aqueous solution. The research demonstrated that amylose could bind quantitatively with metal ions when the ions were at low concentrations.

Although there are a number of publications describing the removal of heavy metal ions from aqueous solution by utilizing xanthated, phosphorylated, or ammoniated starch (Dong et al., 2010; Guo, Sun, Li, Liu, & Ji, 2009; Xu, Wu, Chang, & Zhang, 2010) as well as starch that had been modified with copolymers (Chang, Hao, & Duan, 2008), the use of amylose to remove metal ion through the current strategy has never been reported. This report not only helps to provide an understanding of the induced-assembly mechanism of biomacromolecules, but also provides an alternative strategy for the recovery of precious metals from aqueous solutions and the remediation of water pollution.

2. Experimental

2.1. Materials and reagents

Amylose ($(C_6H_{10}O_5)_n$, was purified from potato starch (which was purchased from Tianjin Ruijinte Chemical Reagent Co. Ltd., China, >99%) in the following manner: the original starch sample was dissolved in dry DMSO at a concentration of 50 mg/mL before it was centrifuged at $2000 \times g$ for 5 min to remove any insoluble impurities. Ethanol was subsequently added to the supernatant to precipitate the amylose, which was dried under high vacuum for 72 h. The amylose was characterized via size exclusion chromatography (SEC), using narrowly dispersed polyethylene glycol samples as a calibration standards and water as a mobile phase. The SEC characterization revealed that the amylose samples possessed a M_w of 13,610 g/mol and a M_w/M_n of 4.55. $CuCl_2{\cdot}2H_2O$ (Tianjin Kemiou Chemical Reagent Co. Ltd., China, >97%), $FeCl_3{\cdot}6H_2O$ (Tianjin Fuchen Reagent Factory, China, >99%), $CdCl_2{\cdot}H_2O$ (Tianjin Fuchen Reagent Factory, China, >99%), $AgNO_3$ (Sinopharm Chemical Reagent Co. Ltd., China, ≥99.8%), and $AlCl_3$ (Tianjin Jinhuitaiya Chemical Reagent Co. Ltd., China, >99.8%) were used as received. All solvents were of analytical grade and used as received, unless indicated otherwise. Pyrene (Aladdin Reagent Co., 97%) was repeatedly crystallized with a solvent mixture consisting of petroleum ether and ethanol before usage. Doubly distilled water was prepared using a home-made water purification system.

2.2. Preparation of the amylose solutions

0.25 g of amylose (containing 0.0046 mol of hydroxyl groups as calculated by expression: $3 \times W_{amylose}/M_{glucose}$ here, W is the weight of amylose, and M is the molecular weight of glucose units of amylose) and 100 mL of distilled water were mixed together before this mixture was magnetically stirred and heated at $100 \pm 1\,^{\circ}C$ to yield a transparent solution, and then preserved at room temperature prior to use. The concentration of the amylose in this solution was 2.5 mg/mL, while the concentration of the hydroxyl groups ([—OH]) of the amylose was 0.046 M.

2.3. Preparation of the metal ion solution

4.3081 g of $CuCl_2$ was dissolved in doubly-distilled water in a 50 mL of volumetric flask, thus yielding an aqueous $CuCl_2$ solution with a concentration of 0.5054 M. $FeCl_3$, $CdCl_2$, $AgNO_3$, and $AlCl_3$ aqueous solutions with various predesigned concentrations were prepared in a similar manner.

2.4. Cu^{2+} induced-assembly of amylose

4.6 mL amylose solutions were transferred into six 10 mL vials. Subsequently, 0.013, 0.05, 0.1, 0.2, 0.4 or 1.6 mL of the $CuCl_2$ solutions were added into the different respective vials before the contents were stirred for 30 min at $70 \pm 1\,^{\circ}C$ to yield stable light blue solutions.

2.5. Characterization of the metal ion induced-assemblies

Transmission electron microscopy (TEM) was performed using a JEM-100 CXII-TEM system that was operated at 80 KeV. Samples were prepared by drying a droplet (10 μL, 1 mg/mL) of the solution on a copper grid that was coated with acetylcellulose membrane. The grid was finally dried overnight in a desiccator before TEM observation. The average size of the assemblies was evaluated from TEM images for more than 200 particles. Fluorescence spectra (FL) were measured using an F-4600 fluorescence spectrophotometer (Shimadzu) at room temperature. Pyrene was dissolved in acetone at a concentration of 6×10^{-7} M before 10 μL of above solution was added into the analysis samples. High purity nitrogen was bubbled to remove trace acetone and dissolved oxygen. 2.5 mL of each sample was placed in a quartz cell with a 1 cm path length to obtain fluorescence emission spectra. The fluorescence excitation wavelength was 334 nm, and the range of the emission wavelengths was 340–760 nm. The UV–vis absorption spectra were measured using a UV–vis–NIR spectrophotometer (UV-8000, Shimadzu). The size and size distribution of assemblies were determined by Dynamic Lighter Scattering (DLS) performed on a 90 plus system (Brookhaven Instruments Corporation, USA). Samples were filtered with a 0.45 μm filter membrane before DLS

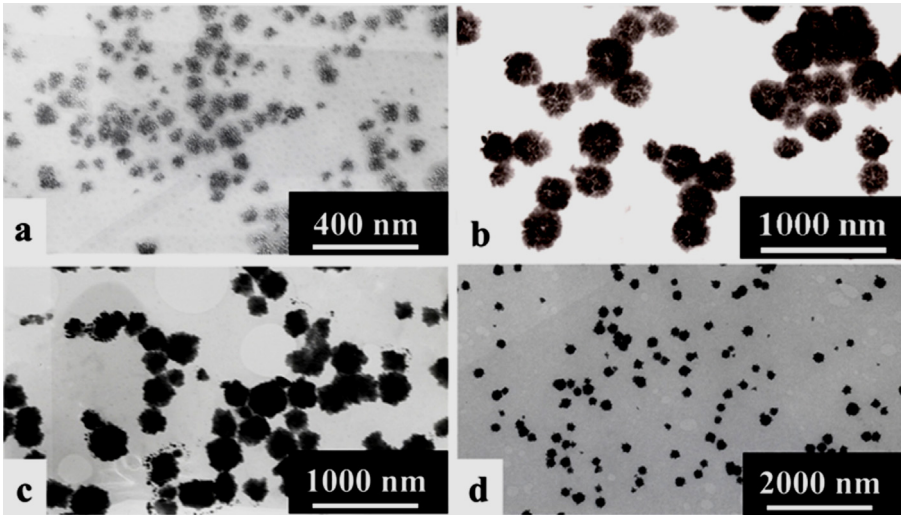

Fig. 1. TEM images of the amylose/Cu^{2+} assemblies that were observed at [Cu^{2+}]/[—OH] ratios of (a) 0.1174, (b) 0.4695, (c) 0.9390, and (d) 3.7559. The molar ratio of Cu^{2+} ions to the hydroxyl group of amylose was denoted as [Cu^{2+}]/[—OH].

measurements. The hydrodynamic radius (D_h) and its polydisperisity index (PDI) were reported based on peak intensity. ^1H NMR spectra were recorded at room temperature using a Bruker DMX-400 spectrometer, with samples dissolved in either D_2O or DMSO-d_6. The concentration of the samples was 1–3 wt%.

2.6. Use of other metal ions to induce amylose assembly

4.6 mL aqueous amylose solutions at 2.5 mg/mL (or [—OH] = 0.5054 M) were transferred into four 10 mL vials, and stirred in an oil-bath at 70 ± 1 °C for 12 h, before aqueous solutions (0.2 mL) of $FeCl_3$, $CdCl_2$, $AgNO_3$ and $AlCl_3$ with predesigned concentrations were added, respectively to the respective vials. The final concentration of the metal ion ([M]) to the concentration of the hydroxyl groups of amylose ([—OH]), [M]/[—OH] was set at 0.4695, 0.2347, and 0.0305, respectively. Stable dispersed solutions of amylose were obtained after the solutions had been stirred for 30 min.

2.7. Capture of metal ions by amylose

Aqueous amylose solutions (at [—OH] = 0.5054 M) were transferred into 10 mL vials, and then mixed with aqueous $CdCl_2$, $FeCl_3$, $CuCl_2$ and $AlCl_3$ solutions with predesigned concentrations, thus yielding solutions with final [M]/[—OH] ratios of 0.01, 0.1, 0.2, 0.5, and 1 for each metal ion/amylose system. The electrical conductivity was determined right after the addition of the metal ions into the amylose solutions, and this value was denoted as σ_0. The electrical conductivity eventually reached a constant value (denoted as σ_1) after the aqueous amylose/metal ion solutions had been stirred at 70 ± 1 °C for 2 h. The variation of the electronic conductivity ($\Delta\sigma$) after addition of metal ions was expressed as $\sigma_0 - \sigma_1$. The ability of the amylose to capture metal ions was an inverse of the percentage of metal ions in the free state, which was expressed as $(\Delta\sigma/\sigma_0) \times 100\%$.

3. Results and discussion

3.1. Cu^{2+} induced-assembly of amylose

The amylose solution turned blue after the addition of the $CuCl_2$ solution. In addition, the path of a laser beam was clearly visible when the laser was directed at the solution. In contrast, this physical phenomenon was absent among solutions consisting solely of $CuCl_2$ or amylose. This behavior provided evidence that the amylose underwent formation of aggregates, which was further confirmed by the TEM images shown in Fig. 1. From these images, it was apparent that amylose self-assembled into spherical assemblies in the presence of Cu^{2+} ions.

In order to further clarify that the spherical assemblies were formed upon the introduction of Cu^{2+} ions rather than consisting solely of amylose aggregates, droplets of the amylose solution were dried on a copper grid and either stained with uranyl acetate (2 wt% in water) prior to TEM observation, or alternatively characterized via TEM without being stained. In both cases, no particles were observed via TEM observation. These results indicated that the formation of these spherical assemblies was indeed induced by the addition of the Cu^{2+} ions to the aqueous amylose solution.

3.2. TEM and DLS analysis of the assemblies in the presence of Cu^{2+} ions at various concentrations

In order to study the mechanism of the self-assembly of amylose in the presence of the Cu^{2+} ions, we investigated the influence of the Cu^{2+} ion concentration on the self-assembly of amylose. The molar ratio of Cu^{2+} ions to amylose was varied by adding different amounts of the $CuCl_2$ solution to the amylose solution, which was kept at a constant concentration. Correspondingly, the [Cu^{2+}]/[—OH] values varied. The TEM images of the amylose/Cu^{2+} assemblies that were observed at various [Cu^{2+}]/[—OH] ratios are shown in Fig. 1.

The TEM diameters of the amylose assemblies observed at different [Cu^{2+}]/[—OH] ratios are shown in Table 1. Amylose assemblies with a diameter of 66 ± 12 nm were formed at a [Cu^{2+}]/[—OH] ratio of 0.1174. As the [Cu^{2+}]/[—OH] ratio increased, the assemblies remained spherical but the diameters of the particle

Table 1
Particle sizes of the amylose assemblies observed with various concentrations of Cu^{2+} ions.

[Amylose] ($\times 10^{-5}$ M)	[Cu^{2+}]/[—OH]	D_h (nm)	PDI	D_{TEM} (nm)
1.4535	0.1174	85	0.232	66 ± 12
1.3953	0.2347	175	0.238	158 ± 32
1.3953	0.4695	290	0.240	286 ± 32
1.3372	0.9390	292	0.245	286 ± 22
1.1046	3.7559	220	0.253	218 ± 26

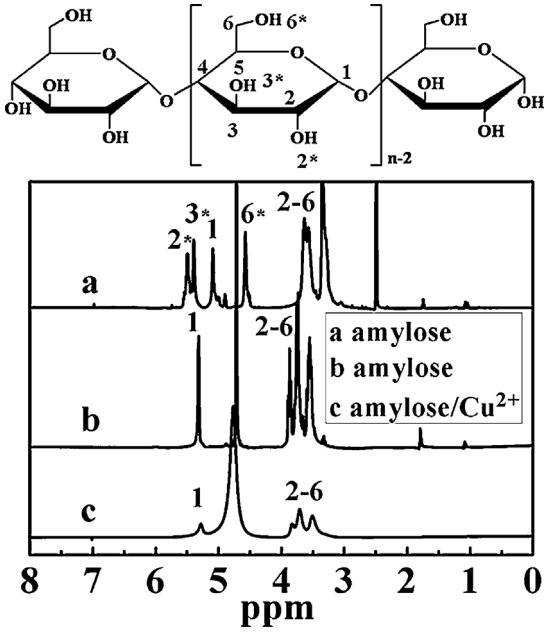

Fig. 2. ^{1}H NMR spectra of amylose and amylose/Cu^{2+} assemblies, including spectra of (a) amylose (DMSO-d_6), (b) amylose (D_2O), and (c) Cu^{2+}/amylose (D_2O).

increased. For example, when the [Cu^{2+}]/[—OH] ratio was increased from 0.1174 up to 0.9390, the diameters of the amylose assemblies increased from 66 ± 12 nm to 286 ± 32 nm, which was in agreement with results that we had reported previously (Li et al., 2013). However, the diameters of the amylose assemblies underwent a converse change, decreasing from 286 ± 32 nm to 218 ± 26 nm, as the [Cu^{2+}]/[—OH] ratio was increased further increased 0.9390 to 3.7559. This phenomenon was mainly due to the decrease of the amylose concentration with the continuous addition of the $CuCl_2$ solution (Table 1). Through careful observation of the spherical assemblies, we found that the appearance of the assemblies changed from the black and white spherical "loose" particles (Fig. 1a) to black spherical "compact" particles (Fig. 1d) as the [Cu^{2+}]/[—OH] ratio was increased. This change may have resulted from more Cu^{2+} ions becoming adsorbed by the amylose as at higher [Cu^{2+}]/[—OH] ratios.

The DLS diameter (D_h) and distribution (PDI) of the amylose assemblies at various [Cu^{2+}]/[—OH] ratios are also shown in Table 1. The D_h initially increased and subsequently decreased with increase in the [Cu^{2+}]/[—OH] ratio. When the [Cu^{2+}]/[—OH] ratio was 0.1174, 0.2347, 0.4695, and 0.9390, the corresponding D_h values were 85, 175, 290, and 292 nm, respectively. As more Cu^{2+} ions were added and the [Cu^{2+}]/[—OH] increased to 3.7559, the D_h decreased to 220 nm. The observation by DLS results was in accordance with the TEM analysis. It is worth noting that results characterized by both DLS and TEM all showed wide particle size distributions (Table 1), which was mainly due to the wide molecular weight distribution (M_w/M_n = 4.55) of amylose.

3.3. *^{1}H NMR and fluorescence investigations on the self-assembly of amylose in the presence of Cu^{2+} ions at various concentrations*

^{1}H NMR spectra of amylose and its assemblies were recorded in different deuterated solvents, as shown in Fig. 2. Amylose was fully soluble in DMSO-d_6, and the major resonance signals observed for amylose were consistent with those that would be anticipated based on the chemical structure (Fig. 2a). The signal at 5.0–5.1 ppm corresponded to the terminal glucose proton (1) at the ends of the amylose chains. Meanwhile, the signal observed at 3.0–3.8 ppm

Table 2
Integral area ratio of amylose and Cu^{2+}/amylose in D_2O.

Sample	H(1) δ/ppm	H(2–6) δ/ppm	Integral area ratio $A_{H(2-6)}/A_{H(1)}$
Amylose/D_2O	5.1–5.3	3.1–3.9	6.1
Cu^{2+}/amylose/D_2O	5.1–5.3	3.1–3.9	4.0

was attributed to other protons of glucose (2–6), 5.3–5.6 ppm and 4.5–4.8 ppm were attributed to the proton signal of hydroxyl groups (2*, 3*, and 6*), while the signals observed at 3.3 ppm and 2.5 ppm corresponded to the protons of H_2O and DMSO-d_6, respectively (Schmitz, Dona, Castignolles, Gilbert, & Gaborieau, 2009).

The ^{1}H NMR spectra of amylose and its assemblies in D_2O are shown in Fig. 2b and c, respectively. The hydroxyl group protons, which exhibited signals in DMSO-d_6, were no longer visible in the spectra shown Fig. 2b and c, which were recorded in D_2O. Meanwhile, the signal corresponding to the terminal glucose protons, exhibited a downfield shift to 5.2–5.4 ppm (Ju et al., 2012; De Graaf, Lammers, Janssen, & Beenackers, 1995). Furthermore, it was apparent that the proton signals of glucose exhibited a change from a doublet to a triplet. In addition, the signal observed at 4.5–4.7 ppm was attributed to D_2O. When the signals of protons 1 and 2–6 in the glucose ring observed in Fig. 2b and c were compared, it was apparent that those observed in Fig. 2c were broadened. This broadening could be attributed to the binding of the Cu^{2+} ions with the hydroxyl groups of amylose.

The ratio of the signal integrations corresponding to the protons H(2–6) and H(1) of glucose (denoted as $A_{H(2-6)}/A_{H(1)}$) was determined, and these ratios are shown in Table 2. This ratio was 6.1 in D_2O, which was close to the theoretical value. However, after the addition of the $CuCl_2$ solution, the ratio changed to 4.0 in D_2O, which indicated that the integrations of the hydroxyl protons (δ = 3–4 ppm) had decreased.

Fluorescence spectroscopy provides an effective method to investigate the assembly behavior of polymers. Pyrene is a common hydrophobic molecular probe that has been used in this field (Winnik, Winnik, Tazuke, & Ober, 1987). The results of the fluorescence spectroscopy analysis using pyrene as a fluorescent probe to investigate the amylose assemblies at different concentrations of Cu^{2+} ions are shown in Fig. 3. Changes in the fluorescence spectra of the amylose assemblies were observed as the concentration of the Cu^{2+} ions was increased. Four fluorescence signals located at 373, 384, 415 and 460 nm were observed when an excitation wavelength of 334 nm was used. The fluorescence intensity ratio I_1/I_3 observed between the first vibronic peak of pyrene (λ = 373 nm) and the third vibronic peak of pyrene (λ = 384 nm) could be used to characterize the variation of the hydrophilic and hydrophobic

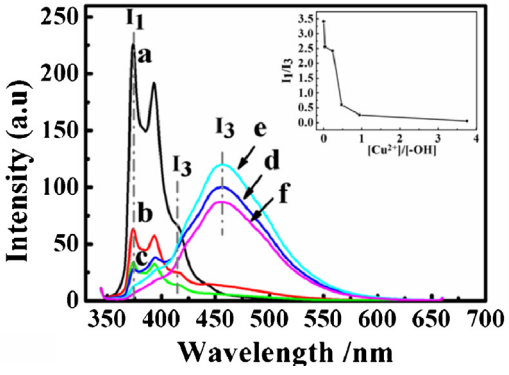

Fig. 3. Fluorescence spectra of amylose assemblies that were formed at various [Cu^{2+}]/[—OH] ratios, including (a) 0.0000, (b) 0.0305, (c) 0.2347, (d) 0.4695, (e) 0.9390, and (f) 3.7559.

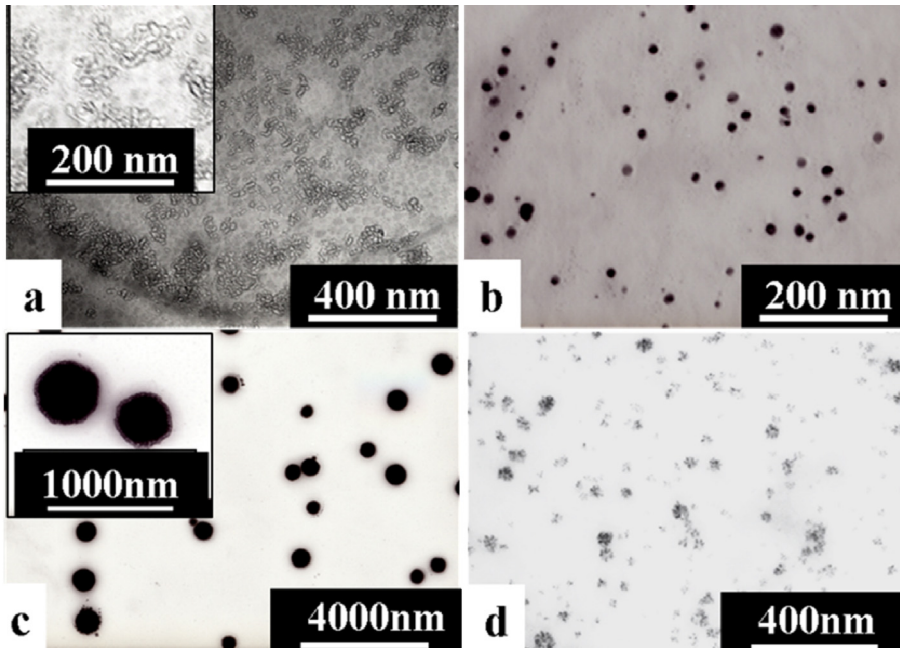

Fig. 4. TEM images of amylose assemblies that were formed in the presence of various metal ions, including (a) Fe^{3+}, (b) Ag^{+}, (c) Al^{3+}, and (d) Cd^{2+}. In all of these cases, the ratio of the metal ion concentration ([M]) to the concentration of the hydroxyl groups of amylose ([—OH]) (denoted as [M]/[—OH]) was 0.4695.

environments of the assemblies. From the illustration in Fig. 3, it was apparent that I_1/I_3 gradually decreased as $[Cu^{2+}]/[—OH]$ was increased, and subsequently leveled off with further increases of $[Cu^{2+}]/[—OH]$. This trend indicated that the hydrophobic domains originated from the interaction between the amylose molecules and Cu^{2+} ions, and that more hydrophobic domains were created as the $[Cu^{2+}]/[—OH]$ ratio was increased. Accordingly, this phenomenon suggested that pyrene gradually transferred from the aqueous phase to the hydrophobic domain. It was worth noting that as the $[Cu^{2+}]/[—OH]$ ratio was increased, the intensities of the signals observed at 415 nm and 460 nm decreased and increased, respectively. The trends exhibited by these two fluorescence emission signals may be attributed to interactions between the amylose hydroxyl groups and the Cu^{2+} ions, which warrant further investigation. The results of this fluorescence spectroscopy investigation demonstrated that the interaction originated from a complexation effect and/or bridging effect between the hydroxyl groups of amylose and the Cu^{2+} ions, thus inducing the assemblies to undergo a hydrophilic-to-hydrophobic transition of the assemblies. Similar assembly formation behavior has been observed by previous researchers via TEM characterization (Hojo, Shirai, & Hayashi, 1974).

3.4. Formation of amylose assemblies in the presence of other metal ions

The directed assembly behavior of amylose was also investigated by using other metal ions to induce the assembly formation. TEM images of amylose assemblies that had undergone complexation with metal ions having different valencies are shown in Fig. 4. Different assembly structures were obtained through when Fe^{3+}, Ag^{+}, Al^{3+} and Cd^{2+} ions were used to induce the assembly of amylose.

When Fe^{3+} ions were used (with $[Fe^{3+}]/[—OH] = 0.4695$), short nanotube-like assemblies were obtained, which featured a white central domain with a diameter of 8 nm, which was surrounded by a black shell with a width of 6 nm. The central white domain was attributed to regions of the amylose that had not undergone interaction with Fe^{3+}, while the black shell was attributed to domains of the amylose that had interacted with the Fe^{3+} ions (Fig. 4a). The formation of the short nanotube-like assemblies indicated that amylose exhibited weak interactions with the Fe^{3+} ions. Meanwhile, as the $[Fe^{3+}]/[—OH]$ ratio was decreased, the diameters of the short nanotube-like assemblies decreased and shells became lighter in color, indicating that fewer Fe^{3+} ions had become bound to the amylose molecules. When the $[Fe^{3+}]/[—OH]$ ratio was decreased to 0.0305, the diameter of the central white domain leveled off, but the width of the black shell diminished to 2–3 nm.

Spherical assemblies with a diameter of ~16 nm were obtained at a $[Ag^{+}]/[—OH]$ ratio of 0.4695 (Fig. 4b). The diameters of the spherical assemblies became smaller with decreases in the $[Ag^{+}]/[—OH]$ ratio. The diameter of the spherical assemblies decreased from 10 to 5 nm when the $[Ag^{+}]/[—OH]$ ratio was decreased from 0.2347 to 0.0305.

In the presence of Al^{3+} ions, nanospheres with a diameter of ~500 nm were obtained when the $[Al^{3+}]/[—OH]$ ratio equaled 0.4695 (Fig. 4c). Meanwhile, the diameters of the nanospheres became smaller as the $[Al^{3+}]/[—OH]$ ratio was decreased. For example, the diameter of the nanospheres was only ~20 nm when the $[Al^{3+}]/[—OH]$ ratio was decreased to 0.0305.

More interestingly, flower-like assemblies were obtained when Cd^{2+} ions were used to induce the assembly of amylose (Fig. 4d). The diameter of the flower-like assemblies was ~40–50 nm at a $[Cd^{2+}]/[—OH]$ ratio of 0.4695. However, no assemblies were observed when the $[Cd^{2+}]/[—OH]$ ratio was decreased to 0.0305, which indicated that Cd^{2+} ions exhibited relatively weaker interactions with amylose.

3.5. Proposed mechanism for the metal ion-induced assembly of amylose

The formation and structure of the Cu^{2+}/amylose assemblies were proposed, and shown in Fig. 5A. Supporting evidence for this proposed mechanism was further proved by UV–vis spectroscopy. UV–vis absorption spectroscopy provides an effective method for probing the interactions between polymers and metal ions (Godard, Wertz, Biebuyck, & Mercier, 1989). The UV–vis absorption

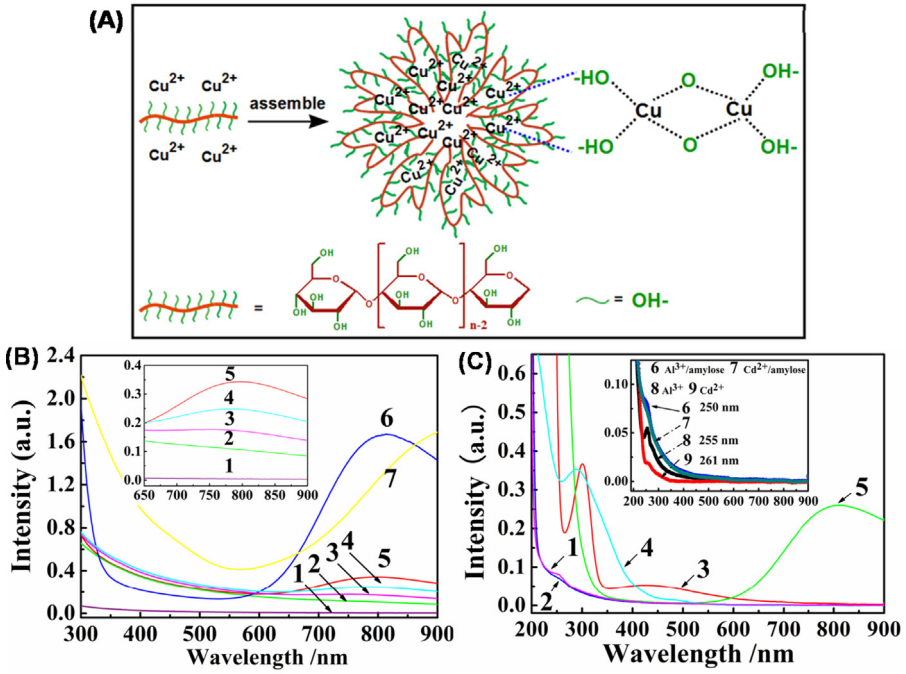

Fig. 5. (A) Formation and structure of the Cu^{2+}/amylose assembly. (B) UV–vis spectra of (1) an aqueous amylose solution, as well as Cu^{2+}/amylose solutions with (2) $[Cu^{2+}]/[—OH] = 0.0305$, (3) $[Cu^{2+}]/[—OH] = 0.2347$, (4) $[Cu^{2+}]/[—OH] = 0.4695$, (5) $[Cu^{2+}]/[—OH] = 0.939$, and (6) $[Cu^{2+}]/[—OH] = 3.7559$. In addition, the spectrum of a $CuCl_2$ solution is also shown in (7). (C) UV–vis spectra of amylose in the presence of various metal ions, including (1) Al^{3+}, (2) Cd^{2+}, (3) Ag^{+}, (4) Fe^{3+}, and (5) Cu^{2+}. The inset image shows the UV–vis spectra of amylose in the presence of (6) Al^{3+}, (7) Cd^{2+}, (8) Al^{3+}, and (9) Cd^{2+} ions.

spectra of aqueous amylose, $CuCl_2$, and Cu^{2+}/amylose solutions (at various Cu^{2+} concentrations) are shown in Fig. 5B.

The amylose solution exhibited no absorption signals in the ultraviolet-visible region, while the $CuCl_2$ solution displayed a large absorption signal at 900 nm. Therefore, the absorption of the $CuCl_2$/amylose solution exhibited an obvious red shift as the concentration of the Cu^{2+} ions was increased. When the $[Cu^{2+}]/[—OH]$ ratios were 0.2347, 0.4695, 0.939 and 3.7559, the corresponding values of λ_{max} were 760, 777, 795 and 813 nm, respectively. This red-shift suggested that the hydroxyl ions of amylose underwent complexation interactions with the Cu^{2+}, which was in agreement with the evidence obtained from the ^1H NMR analysis.

The interactions between amylose and other metal ions were also investigated by UV–vis absorption spectroscopy. The UV–vis absorption spectra of amylose were recorded in the presence of various metal ions, as shown in Fig. 5C. The amylose solution displayed different absorption peaks after the addition of the different metal ions. In particular, the Al^{3+}/amylose, Ag^{+}/amylose, Fe^{3+}/amylose and Cu^{2+}/amylose solutions exhibited absorption signals at 250 (Fig. 5C1), both 299 and 435 nm (Fig. 5C3), 289 (Fig. 5C4), and at 808 nm (Fig. 5C5), respectively. The Cd^{2+}/amylose solution had no obvious UV–vis absorption (Fig. 5C2).

In comparison with the solutions of the free metal ions, the absorptions of the assemblies exhibited a blue shift. For example, the Cu^{2+}/amylose solution displayed an absorption signal at 808 nm, whereas the $CuCl_2$ solution exhibited a strong absorption signal at 900 nm (Fig. 5B7). In addition, the $AlCl_3$ and $CdCl_2$ solutions displayed absorption peaks at 255 and 261 nm, respectively (Fig. 5C8 and C9). However, the absorption signal exhibited by the Al^{3+}/amylose solution shifted to 250 nm, which appeared as a spike instead of as a broad peak (Fig. 5C6). Meanwhile, the Cd^{2+}/amylose solution did not exhibit any significant ultraviolet absorption signals. Interestingly, spherical Ag particles with a diameter of 16 nm were observed after the addition of the silver ions (Fig. 4b). The formation of these Ag particles can be attributed to the reduction of Ag^{+} to Ag, as amylose can behave as a mild reducing agent (Vigneshwaran, Nachane, Balasubramanya, & Varadarajan, 2006). In comparison with the ultraviolet spectrum shown in Fig. 5C3, the Ag^{+}/amylose solution displayed a strong absorption signal at 299 nm, which corresponded to the absorption of free Ag^{+} ions, and this signal was also exhibited by the $AgNO_3$ solution. In addition, the absorption signal observed at 435 nm was attributed to the colloidal Ag particles. The ultraviolet spectra were essentially similar to those reported by Huang et al. (1996) who had prepared Ag particles with a diameter of ~16.2 nm that were dispersed in chloroform. These results suggested that we had obtained Ag/amylose composite particles rather than an Ag^{+}/amylose assembly.

3.6. Capture of metal ions by amylose

The above results demonstrated that amylose could self-assemble in aqueous solution in the presence of various metal ions. On the other hand, metal ions can be captured from aqueous solutions by amylose, which may have practical significance for the recovery of precious metals and may help protect lakes and rivers against spills or pollution. In order to evaluate the ability of amylose to capture various metal ions, its capturing ability was tested against Cd^{2+}, Fe^{3+}, Cu^{2+} and Al^{3+}. During these experiments, the amylose was kept at a constant concentration, and different metal ions solutions with various concentrations were added to the amylose and stirred at $70 \pm 1\,^{\circ}C$ for 2 h. Subsequently, the variation of the electrical conductivity before (σ_0) and after (σ_1) the complexation had occurred between the metal ions and the amylose molecules were measured (Li et al., 2013). The ability of amylose to capture various metal ions was an inverse of the percentage of metal ions in the free state, and was expressed as $(\Delta\sigma/\sigma_0) \times 100\%$ (Fig. 6).

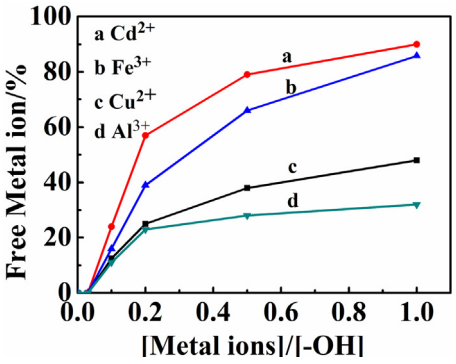

Fig. 6. The ability of amylose to capture different metal ions, including (a) Cd^{2+}, (b) Fe^{3+}, (c) Cu^{2+} and (d) Al^{3+} at various [M]/[—OH] ratios.

The results showed that when the [M]/[—OH] ratio was relatively low, the ability of amylose to capture the metal ions was high, and could reach up to 100%. However, the percentage content of the free metal ions increased at higher [M]/[—OH] ratios, indicating that the capturing ability had diminished under these conditions. Meanwhile, the amylose exhibited different capturing abilities against different metal ions. The ability of amylose to capture different metal ions was as follows: $Cd^{2+} < Fe^{3+} < Cu^{2+} < Al^{3+}$, which was in agreement with the results of TEM analysis.

4. Conclusion

In summary, Cu^{2+}/amylose assemblies with various diameters were prepared through the Cu^{2+} ion induced-assembly of amylose. A preliminary mechanism explaining the metal ion-induced assembly of amylose was also proposed. Spherical assemblies were obtained through a complexation and/or bridging effect between the hydroxyl groups of amylose and the Cu^{2+} ions. Furthermore, the influence of the nature of the metal ion on the morphologies of the resultant metal/amylose assemblies was also investigated. The assembly structures were found to exhibit various morphologies and sizes when different metal ions were used to induce the assembly. In addition, amylose was found to capture the metal ions from aqueous solutions on a quantitative basis, provided that the metal ion solutions were dilute. However, more detailed experiments should be carried out to elucidate the mechanism that underlies the ability of amylose to capture different metal ions and to reveal the factors that may influence these capturing abilities, such as the temperature, pH, and other parameters. The results described in this manuscript have potential applications in the fields of water treatment, separations technology, and for the development of functional nanospheres.

Acknowledgements

We thank the National Natural Science Foundation of China (Nos. 20474068, 51173204, 51203191, 51309074), the Guangdong Natural Science Foundation (S2012010009063), and the Project of the Leading Talents of Guangdong Province for providing financial support. We also thank Dr. Ian Wyman for helping to proofread this paper.

References

Akiyoshi, K., Maruichi, N., Kohara, M., & Kitamura, S. (2002). Amphiphilic block copolymer with a molecular recognition site: Induction of a novel binding characteristic of amylose by self-assembly of poly(ethylene oxide)-*block*-amylose in chloroform. *Biomacromolecules*, *3*, 280–283.

Besheer, A., Hause, G., Kressler, J., & Mader, K. (2007). Hydrophobically modified hydroxyethyl starch: Synthesis, characterization, and aqueous self-assembly into nano-sized polymeric micelles and vesicles. *Biomacromolecules*, *8*, 359–367.

Brown, C. L., Aksay, I. A., Saville, D. A., & Hecht, M. H. (2002). Template-directed assembly of a de novo designed protein. *Journal of the American Chemical Society*, *124*, 6846–6848.

Chang, Q., Hao, X., & Duan, L. (2008). Synthesis of crosslinked starch-graft-polyacrylamide-co-sodium xanthate and its performances in wastewater treatment. *Journal of Hazardous Materials*, *159*, 548–553.

De Graaf, R. A., Lammers, G., Janssen, L. P. B. M., & Beenackers, A. A. C. M. (1995). Quantitative analysis of chemically modified starches by ^{1}H NMR spectroscopy. *Starch*, *47*(12), 469–475.

Dong, A., Xie, J., Wang, W., Yu, L., Liu, Q., & Yin, Y. (2010). A novel method for amino starch preparation and its adsorption for Cu(II) and Cr(VI). *Journal of Hazardous Materials*, *181*(1-3), 448–454.

Godard, P., Wertz, J. L., Biebuyck, J. J., & Mercier, J. P. (1989). Polyvinyl alcohol copper (II) complex – Characterization and practical applications. *Polymer Engineering and Science*, *29*(2), 127–133.

Guo, L., Sun, C., Li, G., Liu, C., & Ji, C. (2009). Thermodynamics and kinetics of Zn(II) adsorption on crosslinked starch phosphates. *Journal of Hazardous Materials*, *161*(1), 510–515.

Han, J., Borjihan, G., Bai, R., Chen, X., & Jing, X. (2008). Synthesis and characterization of starch piperinic ester and its self-assembly of nanospheres. *Journal of Applied Polymer Science*, *108*(1), 523–528.

Hojo, N., Shirai, H., & Hayashi, S. (1974). Complex formation between poly(vinyl alcohol) and metallic ions in aqueous solution. *Journal of Polymer Science*, *47*(1), 229–307.

Huang, H. H., Ni, X. P., Loy, G. L., Chew, C. H., Tan, K. L., Loh, F. C., et al. (1996). Photochemical formation of silver nanoparticles in poly(*N*-vinylpyrrolidone). *Langmuir*, *12*, 909–912.

Ju, B., Yan, D., & Zhang, S. (2012). Micelles self-assembled from thermoresponsive 2-hydroxy-3-butoxypropyl starches for drug delivery? *Carbohydrate Polymers*, *87*(2), 1404–1409.

Li, Y., Gong, Y. K., & Nakashima, K. (2002). Nanoaggregate formation of poly(ethylene oxide)-*b*-polymethaerylate copolymer induced by alkaline earth metal ion binding. *Langmuir*, *18*, 6727–6729.

Li, Y. H., Hu, J. W., Liu, G. J., Zhang, G. W., Zou, H. L., & Shi, J. H. (2013). Amylose-directed synthesis of CuS composite nanowires and microspheres. *Carbohydrate Polymers*, *92*(1), 555–563.

Miles, M. J., Morris, V. J., Orford, P. D., & Ring, S. G. T. (1985). The roles of amylose and amylopectin in the gelation and retrogradation of starch. *Carbohydrate Research*, *135*(2), 271–281.

Moffitt, M., & Eisenberg, A. (1997). Scaling relations and size control of block ionomer microreactors containing different metal ions. *Macromolecules*, *30*, 4363–4373.

Perez, J. M., Simeone, F. J., Saeki, Y., Josephson, L., & Weissleder, R. (2003). Viral-induced self-assembly of magnetic nanoparticles allows the detection of viral particles in biological media. *Journal of the American Chemical Society*, *125*, 10192–10193.

Rosler, A., Vandermeulen, G. W. M., & Klok, H. A. (2001). Advanced drug delivery devices via self-assembly of amphiphilic block copolymers. *Advanced Drug Delivery Reviews*, *53*, 95–108.

Shen, H. W., Zhang, L. F., & Eisenberg, A. (1999). Multiple pH-induced morphological changes in aggregates of polystyrene-*block*-poly(4-vinylpyridine) in DMF/H_2O mixtures. *Journal of the American Chemical Society*, *121*, 2728–2740.

Sheparovych, R., Sahoo, Y., Motornov, M., Wang, S. M., Luo, H., Prasad, P. N., et al. (2006). Polyelectrolyte stabilized nanowires from Fe_3O_4 nanoparticles via magnetic field induced self-assembly. *Chemistry of Materials*, *18*, 591–593.

Morimoto, N., Ogino, N., Narita, T., Kitamura, S., & Akiyoshi, K. (2007). Enzyme-responsive molecular assembly system with amylose-primer surfactants. *Journal of the American Chemical Society*, *129*, 458–459.

Schmitz, S., Dona, A. C., Castignolles, P., Gilbert, R. G., & Gaborieau, M. (2009). Assessment of the extent of starch dissolution in dimethyl sulfoxide by ^{1}HNMR spectroscopy. *Macromolecular Bioscience*, *9*, 506–514.

Tan, Y., Xu, K., Li, L., Liu, C., Song, C., & Wang, P. (2009). Fabrication of size-controlled starch-based nanospheres by nanoprecipitation. *ACS Applied Materials and Interfaces*, *1*, 956–959.

Tan, Y., Xu, K., Li, Y., Sun, S., & Wang, P. (2010). A robust route to fabricate starch esters vesicles. *Chemical Communications*, *46*, 4523.

Vigneshwaran, N., Nachane, R. P., Balasubramanya, R. H., & Varadarajan, P. V. (2006). A novel one-pot 'green' synthesis of stable silver nanoparticles using soluble starch. *Carbohydrate Research*, *341*, 2012–2018.

Wang, Y. C., Tang, L. Y., Li, Y., & Wang, J. (2009). Thermoresponsive block copolymers of poly(ethylene glycol) and polyphosphoester: Thermo-induced self-assembly, biocompatibility, and hydrolytic degradation. *Biomacromolecules*, *10*, 66–73.

Wen, H. S., Cao, J., Wang, L., Chen, Y. W., & Luo, X. L. (2011). Selfassembly of hydrophobic star-branched PCL and PCL-*b*-PEG amphiphilic copolymers. *Acta Polymerica Sinica*, 240–245.

Winnik, F. M., Winnik, M. A., Tazuke, S., & Ober, C. K. (1987). Synthesis and characterization of pyrene-labeled (hydroxypropyl) cellulose and its fluorescence in solution. *Macromolecules*, *20*, 38–44.

Xu, J. P., Ji, J., Chen, W. D., & Shen, J. C. (2005). Novel biomimetic polymersomes as polymer therapeutics for drug delivery. *Journal of Controlled Release*, *107*, 502–512.

Xu, J., Wu, L., Chang, A. C., & Zhang, Y. (2010). Impact of long-term reclaimed wastewater irrigation on agricultural soils: A preliminary assessment. *Journal of Hazardous Materials*, *183*, 780–786.

Zhang, L. F., & Eisenberg, A. (1996). Morphogenic effect of added ions on crew-cut aggregates of polystyrene-*b*-poly(acrylic acid) block copolymers in solutions. *Macromolecules*, *29*, 8805–8815.

Zhang, L. F., Yu, K., & Eisenberg, A. (1996). Ion-induced morphological changes in crew-cut aggregates of amphiphilic block copolymers. *Science*, *272*, 1777–1779.

Zhang, Z. P., Gao, D. M., Zhao, H., Xie, C. G., Guan, G. J., Wang, D. P., et al. (2006). Biomimetic assembly of polypeptide-stabilized $CaCO_3$ nanoparticles. *Journal of Physical Chemistry B*, *110*, 8613–8618.